JACS
JOURNAL OF THE AMERICAN CHEMICAL SOCIETY



Article

# MOF Crystal Chemistry Paving the Way to Gas Storage Needs: Aluminum Based soc-MOF for CH4, O2 and CO2 Storage

Dalal Alezi, Youssef Belmabkhout, Mikhail Suetin, Prashant M. Bhatt, Lukasz Jan Weselinski, Vera Solovyeva, Karim Adil, Ioannis Spanopoulos, Pantelis N. Trikalitis, Abdul-Hamid Emwas, and Mohamed Eddaoudi

*J. Am. Chem. Soc.*, **Just Accepted Manuscript** • DOI: 10.1021/jacs.5b07053 • Publication Date (Web): 14 Sep 2015

# MOF Crystal Chemistry Paving the Way to Gas Storage Needs: Aluminum Based soc-MOF for $CH_4$, $O_2$ and $CO_2$ Storage

Dalal Alezi,[†] Youssef Belmabkhout,[†] Mikhail Suyetin,[†] Prashant M. Bhatt,[†] Łukasz J. Weseliński,[†] Vera Solovyeva,[†] Karim Adil,[†] Ioannis Spanopoulos,[§] Pantelis N. Trikalitis,[§] Abdul-Hamid Emwas,[‡] Mohamed Eddaoudi*,[†]

[†]Functional Materials Design, Discovery and Development Research Group (FMD[3]), Advanced Membranes and Porous Materials Center, Division of Physical Sciences and Engineering, King Abdullah University of Science and Technology (KAUST), Thuwal 23955-6900, Kingdom of Saudi Arabia, E-mail: mohamed.eddaoudi@kaust.edu.sa

[‡]Imaging and Characterization Core Lab, King Abdullah University of Science and Technology (KAUST)

[§]Department of Chemistry, University of Crete, Voutes 71003, Heraklion, Greece

*Supporting Information Placeholder*

**ABSTRACT:** The molecular building block approach was employed effectively to construct a series of novel isoreticular, highly porous and stable, aluminum based Metal-Organic Frameworks with **soc** topology. From this platform, three compounds were experimentally isolated and fully characterized, namely, the parent Al-**soc**-MOF-1 and its naphthalene and anthracene analogues. Al-**soc**-MOF-1 exhibits outstanding gravimetric methane uptake (total and working capacity). It is shown experimentally, for the first time, that the Al-**soc**-MOF platform can address the challenging Department of Energy dual target of 0.5 g/g (gravimetric) and 264 $cm^3$ (STP)/$cm^3$ (volumetric) methane storage. Furthermore, Al-**soc**-MOF exhibited the highest total gravimetric and volumetric uptake for carbon dioxide and the utmost total and deliverable uptake for oxygen at relatively high pressures among all microporous MOFs. In order to correlate the MOF pore structure and functionality to the gas storage properties, to better understand the structure-properties relationship, we performed a molecular simulation study and evaluated the methane storage performance of Al-**soc**-MOF platform using diverse organic linkers. It was found that shortening the parent Al-**soc**-MOF-1 linker resulted in a noticeable enhancement in the working volumetric capacity at specific temperatures and pressures with amply conserved gravimetric uptake/working capacity. In contrast, further expansion of the organic linker (branches and/or core) led to isostructural Al-**soc**-MOFs with enhanced gravimetric uptake but noticeably lower volumetric capacity. The collective experimental and simulation studies indicated that the parent Al-**soc**-MOF-1 exhibits the best compromise between the volumetric and gravimetric total and working uptakes in a wide range of pressure and temperature conditions.

## INTRODUCTION

Gas storage in porous materials is a desirable technology that has been significantly developed in recent years, owing to its potential to address numerous persisting challenges in a number of industrial applications related to energy, environment, and health care sectors.[1] In the context of clean energy, there is an amplified willingness to reduce greenhouse gas emissions, caused by energy production processes, as evident by the considerable ongoing research in academia and industry alike aiming to develop practical solutions to mitigate this problem. Correspondingly, appropriate studies have been conducted in order to practically deploy a relatively cleaner alternative fuels such as methane ($CH_4$), a primary component of natural gas (NG) and biogas. $CH_4$ is of great interest as a fuel for stationary and mobile applications due to (i) its high H to C ratio in comparison to other fossil fuels, resulting in a relatively lower CO and $CO_2$ emissions,[2] and (iii) its lower sulfur and nitrogen contents leading to a lessen $SO_x$ and $NO_x$ emissions. The aforementioned attributes position $CH_4$ as an appreciably cleaner fuel than gasoline and diesel.[3] Nonetheless, the main drawback of $CH_4$, as compared to liquid fossil fuels, is its low volumetric energy density. Therefore development of suitable and sustainable on-board vehicle methane storage solutions, close to room temperature, is vital to the successful deployment of methane as a conventional fuel for transport applications.[4]

Highly porous materials represent an interesting category of adsorbents that display distinct structural advantages for $CH_4$ storage. The appropriate combination of a high surface area associated to a considerable pore volume with a suitable pore shape and functionality, in a given porous material, is crucial to

achieve the desired enhanced $CH_4$ storage uptake and a practical working capacity at a set pressure and temperature.[5] It is to note that the volumetric working capacity is an essential parameter to assess the material's performance towards $CH_4$ storage. The working capacity represents the usable amount of $CH_4$ derived by subtracting the unused adsorbed $CH_4$, corresponding to the uptake at the delivery pressure (5 bar), from the uptake at the maximum adsorption pressure (35 bar or higher).[6] Prominently, one of the pathways to enhance the methane working capacity of a given porous material is to regulate its methane uptake at relatively low pressures and subsequently reduce the unused $CH_4$ uptake up to the 5 bar threshold.

Relatedly, the storage of other gases such as nitric oxide (NO) and carbon dioxide ($CO_2$) has been previously studied and explored for various relevant applications.[1a, 7,8] On the contrary, studies pertaining to high pressure oxygen ($O_2$) storage are still scarce.[9] The availability of high amounts of $O_2$ is of prime importance in health care domain, particularly in the treatment of respiratory insufficiencies and in hyperbaric oxygen changes for the treatment of carbon monoxide poisoning. Correspondingly, large amount of oxygen is used to enrich air during catalysts regeneration in the catalytic cracking units.[10] Markedly, there is a significant need in developing efficient pathways to store $O_2$ for various industrial needs.

Metal Organic Frameworks (MOFs), a special class of solid-state materials, emerged as modular and functional porous materials that can offer potential to address many enduring challenges pertaining to energy and environmental sustainability.[11] Principally, advances in MOF chemistry have permitted the successful implementation of reticular chemistry, predesigned building blocks were directed to assemble into a preset network topology. Namely, the Molecular Building Block (MBB) approach is deployed to construct targeted functional MOFs, where desired structural and geometrical attributes are incorporated into the MBBs prior to the assembly process. In effect, isolating reaction conditions that consistently permit *in situ* formation of the requisite inorganic MBBs, in the presence of a suitable organic linker, is essential for the successful implementation of the MBB approach and the subsequent formation of the targeted MOF with desired network topology.[12]

Advantageously, the MBB approach permits the rational assembly of targeted MOFs and their subsequent structural fine-tuning using isoreticular chemistry.[2b] The deliberate alteration of a MOF dimensionality and functionality without changing its underlying topology, isoreticular chemistry, is regarded as a powerful pathway for the development of new functional materials with distinctive properties.

Evidently, the selection of an appropriate MOF platform, with desired topological attributes for the logical practice of isoreticular chemistry, offers potential to readily access porous materials suitable to address the ongoing gas storage challenges.[11a, 13] Practically, several key requisites are considered and targeted in order to facilitate the attainment of a high storage MOF media: i) inorganic MBBs based on light and abundant elements, ii) organic MBBs amenable to size, shape and functionality adjustments via expansion and decoration, iii) an elect MOF platform that permits access to isoreticular MOFs with concomitant high surface area, large pore volume and fine-tuned pores in the micropore domain, and iv) a MOF platform based on an underlying topology that prohibits interpenetration upon MOF expansion.

In this context and considering the aforementioned requisites, we identified the MOF platform based on the **soc** topology (**s**quare-**oc**tahedral) as a promising platform to access isoreticular MOF materials for potential use in gas storage and separation applications. The **soc**-MOF platform offers interesting structural features where the pore system comprised of cavities and channels can be fine-tuned in the micropore domain by the judiciously fine-tuning the square building unit (the tetra-carboxylate ligand).[14] It is to note, that the first reported **soc**-MOF materials (In, Ga, and Fe based **soc**-MOF) revealed an exceptionally high gas storage density for $H_2$ and $CH_4$[11h, 15] albeit their associated moderate surface area and pore volume when compared to the best storage MOF materials.[6a, 16] Congruently, we found it compelling to target **soc**-MOFs with relatively larger surface areas and pore volumes, via isoreticular chemistry where the expansion strategy is employed to construct isoreticular **soc**-MOFs based on selected/compatible and expanded organic MBBs, and subsequently evaluate their performance for storage of valuable commodities such as $CH_4$, $H_2$, $CO_2$ and $O_2$.

Markedly, the construction of a highly microporous MOF with a **soc** topology requires the judicious selection of an expanded rectangular organic linker that facilitates the *in situ* formation of the targeted inorganic oxo-centered trinuclear M(III) cluster $[M_3(\mu_3\text{-O})(O_2C–)_6]$, ($M^{3+}$= In, Al, Fe, etc.). Specifically, targeting MOFs based on the trinuclear aluminum(III) cluster will permit the development of a relatively low cost material with tailored properties for gas storage applications.[17] It is important to note that MOFs based on trinuclear Al(III) cluster $[Al_3(\mu_3\text{-O})(O_2C–)_6]$, 6-connected MBB, are scarce with only few examples reported in the literature due to challenges in isolating reaction conditions that allow the *in situ* formation of the said inorganic MBB.[18]

In this work, we report the synthesis and the single-crystal structure, based on single-crystal X-ray diffraction (SCXRD) studies, of the first aluminum MOF with the **soc** topology and possessing an exceptional porosity. Importantly, this is the first report disclosing the assembly of the oxo-centered trinuclear aluminum(III) cluster (oxo-centered aluminum(III) trimer), $[Al_3(\mu_3\text{-O})(O_2C–)_6]$, with a quadrangular ligand into a given MOF, namely a highly microporous **soc**-MOF with more than 2 $cm^3/g$ pore volume and 6000 $m^2/g$ apparent Langmuir surface area. Furthermore, the use of similar reaction conditions, that afforded the synthesis of the parent Al-**soc**-MOF-1, in the presence of functionalized tetracarboxylate linkers (with naphthalene or anthracene replacing the phenyl core in the parent ligand) resulted in two new isoreticular structures, namely naphthalene Al-**soc**-MOF-2 and anthracene Al-**soc**-MOF-3. Extensive gas adsorption studies were carried out on these isoreticular **soc**-MOFs with different gases ($N_2$, $CO_2$, $CH_4$, $O_2$) at low pressures (cryogenic temperatures) and at high pressures. In particular, $CH_4$ and $O_2$ adsorption isotherms were investigated experimentally at different temperatures and in a wide range of pressures up to 85 and 120 bar, respectively. It was found that Al-**soc**-MOF-1 have one of the highest ever total and working gravimetric $CH_4$ uptake at 35 bar and higher pressures at any given temperature. In the contrast to all other best MOFs reported to date in the open literature for $CH_4$ storage, the parent Al-**soc**-MOF-1 sorption studies revealed an enhancement in the volumetric $CH_4$ storage working capacity when the temperature was decreased. Particularly, at 258 K and 80 bar, the Al-**soc**-MOF-1 fulfilled the Department of Energy (DOE) targets (both gravimetric and volumetric) and exhibited the highest working volumetric capacity of 264 ($cm^3STP/cm^3$).

Correspondingly, to the best of our knowledge, Al-**soc**-MOF-1 showed the highest gravimetric total capacity for $CO_2$ and $O_2$ among microporous MOFs. Furthermore molecular simulation studies supported and confirmed our experimental results for $CH_4$ storage and thus encouraged us to explore various plausible theoretical isoreticular Al-**soc**-MOFs, based on expanded and/or functionalized tetracarboxylate organic building blocks, for $CH_4$ storage. This study permitted to i) pinpoint various prospective Al-**soc**-MOFs with similar outstanding $CH_4$ storage capabilities as the parent Al-**soc**-MOF-1, confirming the superior storage capabilities of the parent Al-**soc**-MOF-1 both volumetric and gravimetric, ii) gain a better understanding of the structure-properties relationship, deriving a better correlation between the **soc**-MOF gas storage properties and the make-up of the **soc**-MOF porous system (pore shape and size, ligand dimensions and functionalities).

## RESULTS AND DISSCUSION

In our effort to isolate the first aluminum based **soc**-MOF, numerous attempts have been carried out to isolate reaction conditions that consistently allow the formation *in situ* of the desired trinuclear aluminum(III) MBB, $[Al_3(\mu_3\text{-}O)(O_2C\text{–})_6]$. Accordingly, we designed and synthesized 3,3",5,5"-tetrakis(4-carboxyphenyl)-p-terphenyl ($H_4$TCPT) tetratopic ligand (**$H_4$L1**)[19] that can act as a rectangular MBB. Successfully, reactions between **$H_4$L1** and $AlCl_3{\cdot}6H_2O$ in acidic solution containing the mixture of N,N`-dimethylformamide (DMF) and acetonitrile ($CH_3CN$) afforded colorless homogeneous crystals with a cube-shaped morphology, characterized and formulated by SCXRD as $[Al_3O(TCPT)_{1.5}(H_2O)_3]{\cdot}|Cl^-|$ (**1**). Compound **1** crystallizes in the cubic *Pm-3n* space group. The crystal structure of **1** reveals a 3-periodic framework built up from $\mu_3$-oxo-centered trinuclear Al(III) inorganic MBB (oxo-centered Al(III) trimer), $[Al_3(\mu_3\text{-}O)(H_2O)_3(O_2C\text{–})_6]$. Each aluminum cation ($Al^{3+}$) displays an octahedral coordination environment and coordinates to six oxygen atoms, namely, four bis-monodentate deprotonated carboxylate oxygen atoms from four independent $TCPT^{4-}$ ligands, one $\mu_3$-oxo anion and the coordination sphere is completed by a terminal aqua ligand. The trinuclear Al(III) MBBs are bridged by six independent $TCPT^{4-}$ ligands resulting in the formation of a 3-periodic cationic framework, Al-**soc**-MOF-1 (Figure 1). The charge balance is provided by the presence of chloride ions, which is confirmed by the X-ray photoelectron spectroscopy (XPS) experiment (Figure S11, Supporting Information). Crystallographic analysis affirms that the chloride ions are disordered over six positions around the trinuclear Al(III) cluster with equal probability. This analysis was also supported by $^{27}$Al solid state NMR spectroscopy experiment (Figure S12, Supporting Information).

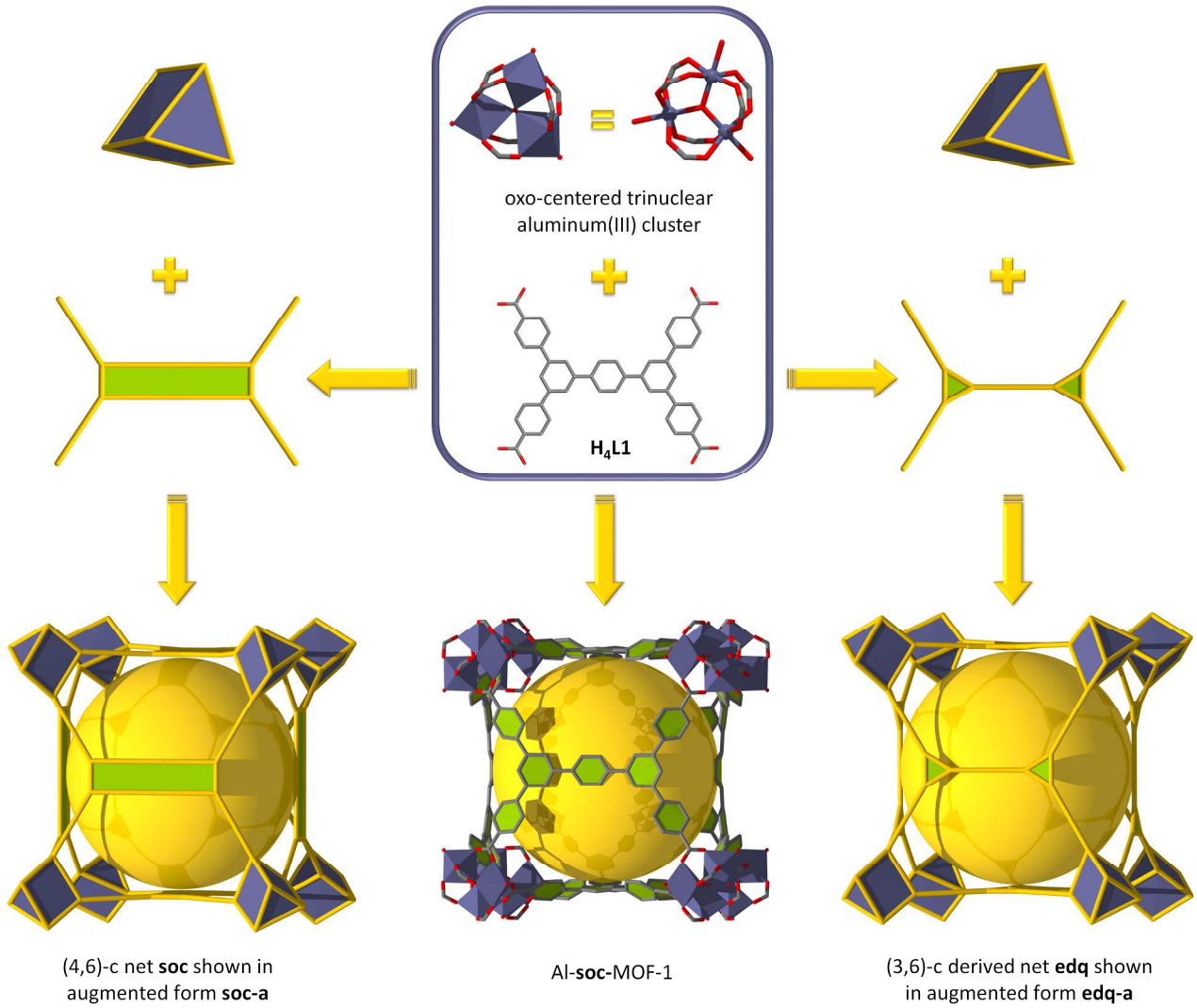


**Figure 1.** Crystal structure of **1** showing the assembly of the trinuclear aluminum(III) MBB, $[Al_3(\mu_3\text{-}O)(H_2O)_3(O_2C\text{–})_6]$, with organic ligand, $H_4TCPT$ (middle). Topological analysis of **1**, where the 6-connected trinuclear Al(III) MBB can be viewed as trigonal prismatic SBU, while the organic ligand can be rationalized as a 4-connected building unit to give (4,6)-c **soc**-net (left), or can be viewed as 3-c SBUs resulting in a (3,6)-c derived net **edq** (right).

Topological analysis reveals that **1** has the anticipated edge transitive (4,6)-connected net with the **soc** underlying topology. The trinuclear Al(III) MBB, $[Al_3(\mu_3\text{-}O)(O_2C\text{–})_6]$, can be regarded a trigonal prism secondary building unit (SBU) with the six points of extension corresponding to the carbon of the carboxylate moieties match the vertex figure of the 6-c node in the **soc** net. The 6-c inorganic MBBs are joined by the rectangular organic ligand, 4-c node, into a primitive cubic system arrangement (Figure 1).[20] Alternatively from topological perspective, the 4-c rectangular ligand can be regarded as comprised of two interconnected 3-c triangular SBUs that are further linked through the 6-c trigonal prismatic SBUs to afford a MOF related to a (3,6)-c derived net **edq**, with transitivity 2 2 (Figures 1, Figures S25 and S26, Supporting Information).[20b,21] However, in this paper, the reported Al-MOFs will be referred to as Al-**soc**-MOFs.

In order to isolate other isoreticular analogs of Al-**soc**-MOF-1, the phenyl ring located in the core of TCPT ligand was substituted by 1,4-naphthalenyl and 9,10-anthracenyl cores to give the naphthalene and anthracene functionalized ligands, 3',3",5',5"-tetrakis(4-carboxyphenyl)-1,4-diphenylnaphthalene (TCDPN) (**$H_4$L2**) and 3',3",5',5"-tetrakis(4-carboxyphenyl)-9,10-diphenylanthracene (TCDPA) (**$H_4$L3**), respectively (Figure 2a).[19] As anticipated, under similar reaction conditions, which were used to isolate the Al-**soc**-MOF-1, cube-shaped crystals were obtained and characterized using SCXRD and powder X-ray diffraction (PXRD) studies (Figure 2b), revealing the construction of two isoreticular Al-**soc**-MOF compounds, naphthalene Al-**soc**-MOF-2 **(2)** and anthracene Al-**soc**-MOF-3 **(3)** with the following formula $[Al_3O(Ligand)_{1.5}(H_2O)_3]\cdot|Cl^-|$.

The phase purity of Al-**soc**-MOF compounds, **1**, **2** and **3**, were confirmed by Whole Profile Pattern Matching using Le Bail method (Figures S13, S14 and S15, Supporting Information).[22]

Al-**soc**-MOF-1 structure encloses cubic shaped cages with 14.3Å in diameter delimited by six $TCPT^{4-}$ ligands, which occupy the faces of the cage, and eight inorganic trinuclear Al(III) clusters located on the vertices of the cuboidal cage. The cage is accessible through apertures of approximately 5.6 × 8.4Å taking van der Waals (vdW) radius into consideration. The structure also encloses two well-defined 1D infinite channels with estimated dimensions of 14Å (vdW), which is approximately at the border of microporous materials. (Figures S23 and S24, Supporting Information).

The corresponding solvent accessible free volumes for **1**, **2** and **3** were estimated to be 80.5 %, 79 % and 75 %, respectively, by summing voxels more than 1.2 Å away from the framework using PLATON software.[23]

**Table 1.** Selected porosity data for Al-**soc**-MOFs compounds. $A_{BET}$, $A_{Lang}$ are the experimental BET and Langmuir specific surface areas. $PV_{theo}$, and $PV_{exp}$ are the calculated pore volume from crystal structures and the experimentally measured pore volume, respectively

| Compound | $A_{BET}$ $m^2/g$ | $A_{Lang}$ $m^2/g$ | Density $g/cm^3$ | $PV_{theo}$ $cm^3/g$ | $PV_{exp}$ $cm^3/g$ |
|---|---|---|---|---|---|
| **Al**-soc-**MOF-1** | 5585 | 6530 | 0.34 | 2.3 | 2.3 |
| **Al**-soc-**MOF-2** | 5162 | 5976 | 0.36 | 2.2 | 2.1 |
| **Al**-soc-**MOF-3** | 4849 | 5212 | 0.38 | 1.9 | 1.8 |

In light of the extraordinarily pure microporous architecture exhibited by **1**, **2** and **3**, optimization of the conventional activation conditions (drying under vacuum and heating) showed that the guest solvent in the pores could be easily removed using traditional approach (vacuum and heating) without altering their microporosity. Nitrogen ($N_2$) adsorption measurements at 77 K were carried out on the acetonitrile exchanged samples, showing fully reversible type-I isotherm representative of porous materials with permanent microporosity (Figure 2c).

The Langmuir and BET specific surface area, in the pressure range (0.015-0.0269 $p/p_0$), were estimated and found to be ca. (6530, 5585 $cm^3/g$) for **1**, (5976, 5161 $cm^3/g$) for **2**, and (5212, 4849 $cm^3/g$) for **3** (Table 1). It is to note that the resultant high microporosity (surface area and pore volume) is exceptional and yet to be observed, prior to this work, using traditional activation method that often causes pore collapse in the case of highly porous MOFs.[24] Such a unique feature is of prime importance for the implementation and deployment of **1**, **2** and **3** as a gas storage media for onboard or stationary gas storage applications.

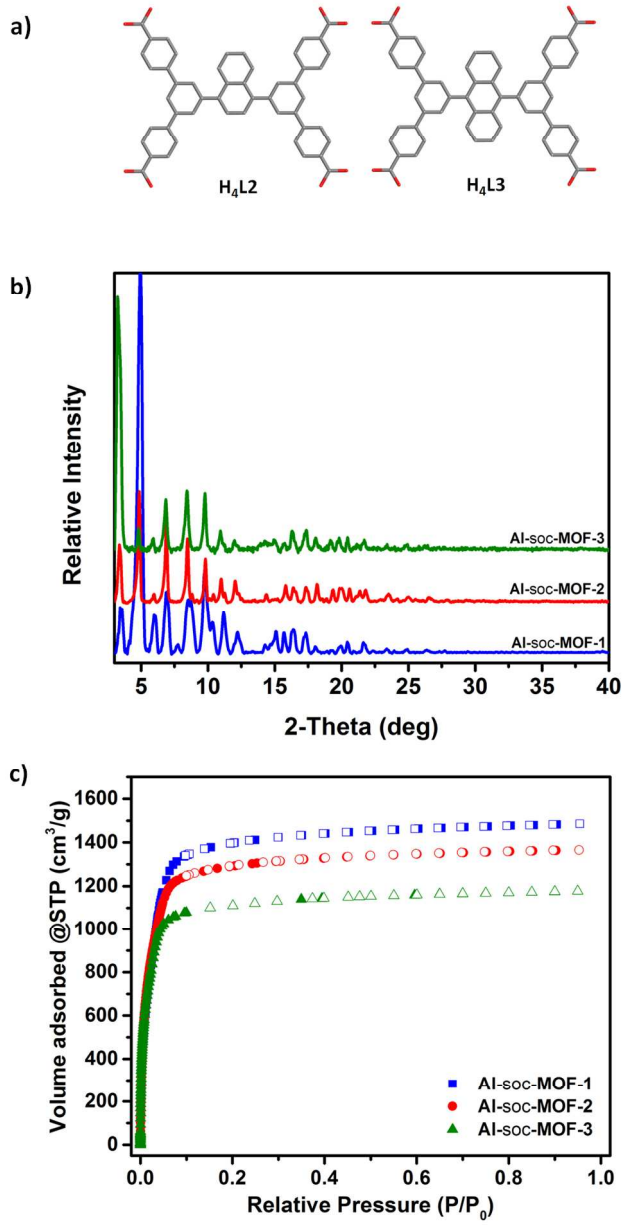


**Figure 2.** (a) Representation of the organic MBBs used to construct isoreticular Al-**soc**-MOFs. (b) PXRD patterns for the isoreticular Al-**soc**-MOFs. (c) Nitrogen isotherms at 77K for the isoreticular Al-**soc**-MOFs.

The successful use of the conventional activation method was confirmed by the excellent agreement between the experimental and the optimal theoretical pore volumes ($PV_{exp}$= 2.3, 2.1 and 1.8 $cm^3/g$, $PV_{theo}$= 2.3, 2.2 and 1.9 $cm^3/g$ for **1**, **2**, and **3,** respectively). Furthermore, Al-**soc**-MOF structures preserved their optimal porosity after heating up to 340 °C under vacuum (Figures S27b, S34b and S36b, Supporting Information), another essential feature that is rarely observed for highly porous MOFs. The high thermal stability was also confirmed using variable temperature PXRD studies and thermal gravimetric analysis (Figures S17- S22, Supporting Information).

**Methane Storage Studies.**

Interestingly, the extremely open structure, exclusively concerted in the microporous range, combined with the distinctive structural features (presence of cages and channels) place Al-**soc**-MOFs as ideal adsorbent candidates for gas storage studies. Accordingly, $CH_4$ adsorption on **1**, **2** and **3** was extensively studied experimentally at variable temperatures and up to 80 bar as well as at low pressure and 112 K (boiling point of $CH_4$).

The methane adsorption isotherms at 112 K for **1**, **2** and **3** revealed remarkable $CH_4$ uptakes near saturation pressures, *e.g.* 1336, 1205 and 1055 $cm^3$ (STP)/g at $p/p_0$ = 0.95, respectively (Figures S28a, S35a and S37a, Supporting Information). Importantly, high pressure $CH_4$ adsorption isotherms at variable temperatures, depicted in Figure 3, showed that **1** has one of the highest ever reported $CH_4$ gravimetric uptakes (ca. 361 $cm^3$(STP)/g) for any microporous MOF materials at the disclosed DOE operational storage conditions (298 K and 35 bar). Mesoporous MOF-210[24b] and DUT-49[25] displayed an uptake around 210 and 364 $cm^3$(STP)/g at the same conditions. Interestingly, the DOE $CH_4$ gravimetric uptake target of 700 $cm^3$ (STP)/g (0.5 g/g) was addressed and reached for relatively high pressures at temperatures below 288 K, *e.g.* 50 bar at 258 K and 85 bar at 288 K (Figure 3).

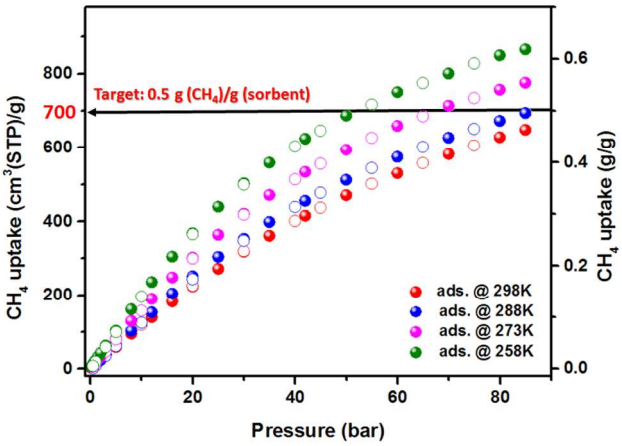


**Figure 3.** Single component gas adsorption isotherms for $CH_4$ at different temperatures for Al-**soc**-MOF-1, showing total $CH_4$ gravimetric uptakes surpassing the DOE target at particular pressures and temperatures.

Additionally, analysis of the volumetric $CH_4$ adsorption isotherms, using the Al-**soc**-MOF-1 crystal density, revealed an enhancement in the volumetric $CH_4$ storage working capacity when the temperature was decreased (Figure 4). Specifically, the volumetric $CH_4$ storage working capacity for **1** increased from 201 $cm^3$(STP)/$cm^3$ to 264 $cm^3$(STP)/$cm^3$ when the temperature was decreased from 298 K to 258 K at working pressures between 80 bar (adsorption) and 5 bar (desorption). This attribute, unique to Al-**soc**-MOF-1, is unprecedented as all available $CH_4$ storage data for MOFs showed the conventional decrease in the volumetric $CH_4$ storage working capacity with the decrease in temperature as illustrated in Figure 4 and Table S3 for UTSA-76,[26] HKUST-1,[16, 27] Ni-MOF-74,[16, 27b, 28] , NU-111[29] and PCN-14.[16, 27b, 30] It is to note that MOF-519[6a] was not included in this comparative assessment as the associated data at low temperatures were not available for this highly $CH_4$ adsorbing MOF.

A comprehensive comparison of absolute $CH_4$ uptakes and working capacities for Al-**soc**-MOF-1 (**1**) with various best MOF materials reported so far at different temperature and pressure conditions is presented in Figures 5 and Figure S38, Supporting Information. Interestingly, although the total volumetric $CH_4$ uptake for **1** is relatively lower than some of the highly adsorbing MOFs, **1** displayed mutually high volumetric and gravimetric working capacities at different working temperatures and pressures. This notable and rare compromise between the gravimetric and the volumetric capacities for **1** is a result of the reduced unused $CH_4$ uptake below 5 bar and the linear trend of the $CH_4$ isotherms at relatively high pressures, a desirable attribute for an appropriate gas storage media. In contrast to the best MOFs reported so far for $CH_4$ storage, **1** exhibits relatively low $CH_4$ heat of adsorption (11 kJ/mol at low loading) in the relatively low $CH_4$ loading region, only slightly higher than the $CH_4$ latent heat of evaporation (Figure S30, Supporting Information). Markedly, the comparatively favorable methane adsorption at relatively high pressures can be attributed to enhanced $CH_4$-$CH_4$ interactions regulated by the appropriate pore size of the Al-**soc**-MOF-1. Therefore, the combination of both aforementioned effects, governing the $CH_4$ adsorption at low and high pressures, in a single material afforded the exceptional $CH_4$ working capacities observed for the Al-**soc**-MOF-1, especially at relatively low temperatures. It is to note that **1** exhibits the second highest $CH_4$ volumetric working capacity at 298 K and 5-80 bar working pressure range, namely 201 $cm^3$ (STP) /$cm^3$ vs. 230 $cm^3$ (STP)/$cm^3$ for the recently reported MOF-519. Noticeably, the two synthesized isoreticular Al-**soc**-MOFs (**2** and **3**) exhibited also high gravimetric and volumetric total and working $CH_4$ uptakes that were only slightly lower than the uptake values derived for **1**. The experimental results for **2** and **3** are summarized in Figure S41 and Table S4, Supporting Information.

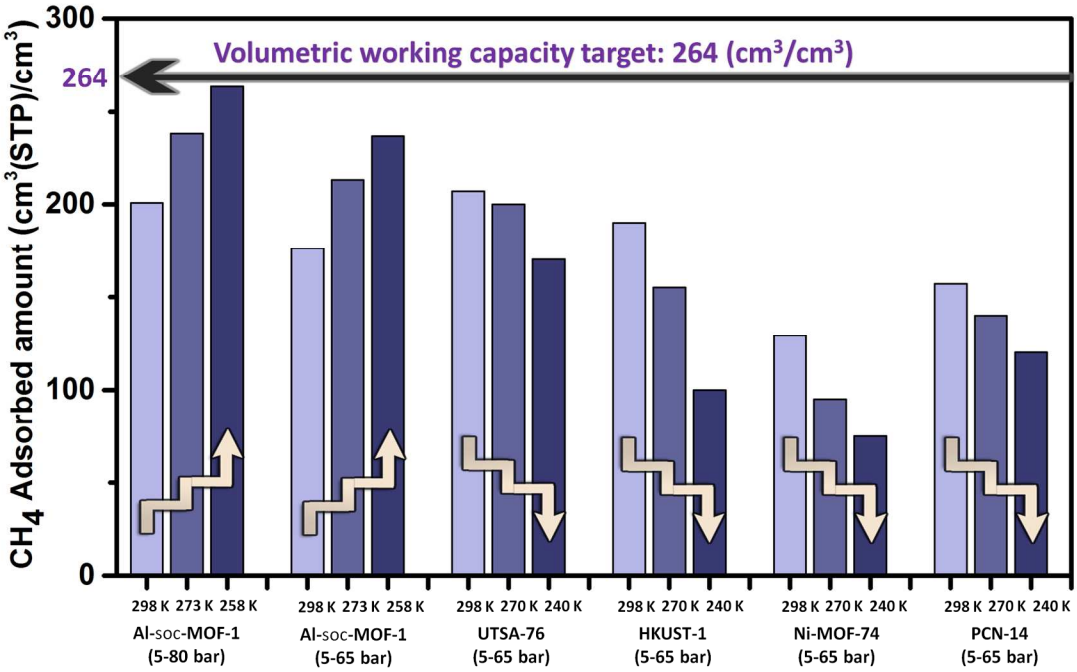


**Figure 4.** Comparison of the $CH_4$ volumetric working capacities (5-80 bar and 5-65 bar) at different temperatures (258, 273 and 298K) for Al-**soc**-MOF-1 with the best microporous MOF materials reported to date.

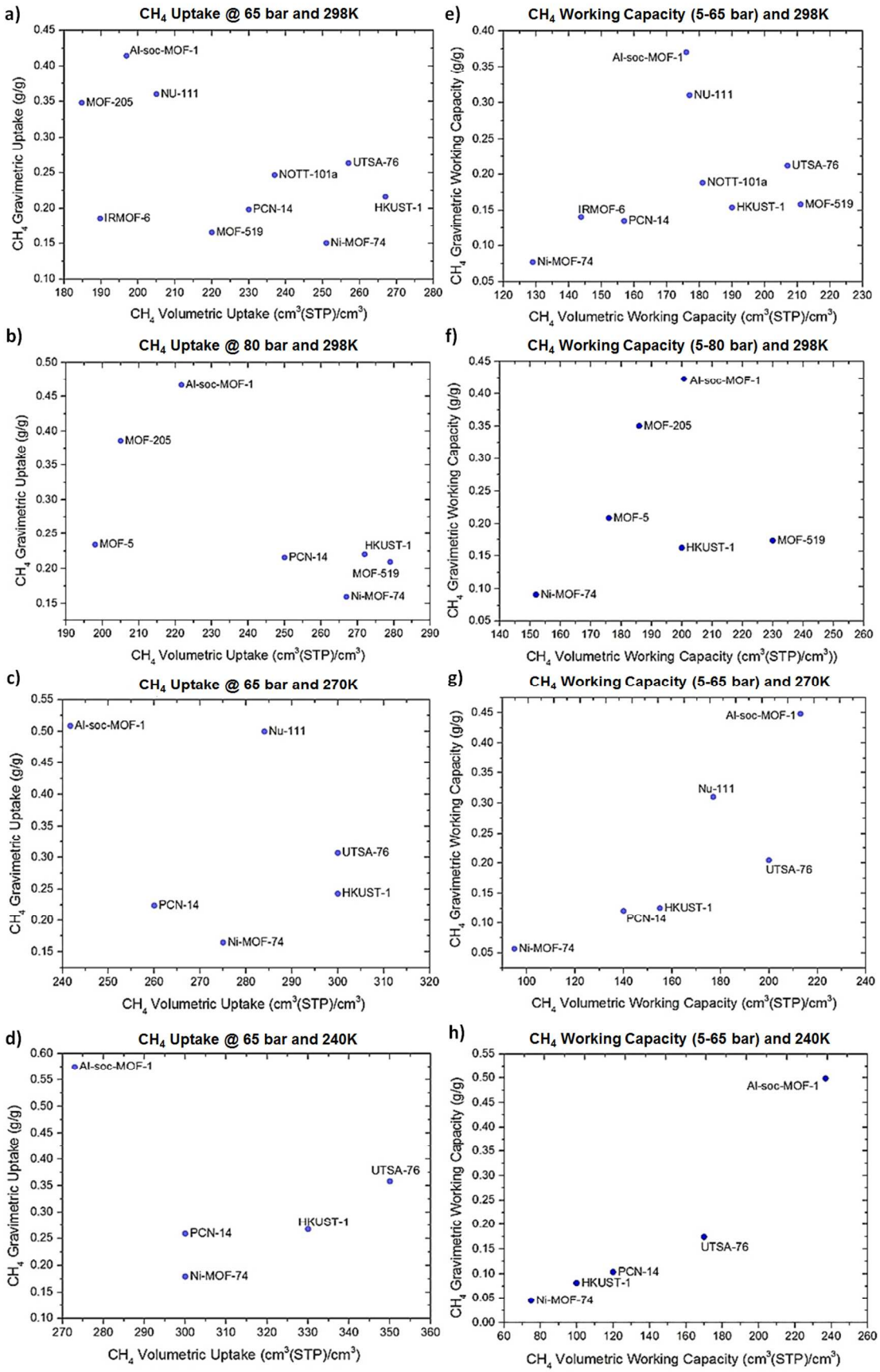


**Figure 5.** Total (a, b, c, d) at 65 and 80 bar and 5-65, 5-80 bar working (e, f, g , h) $CH_4$ gravimetric and volumetric uptakes for Al-**soc**-MOF-1 **(1)** as compared to the best MOF materials reported to date at 298, 270 and 240 K. The data for the Al-**soc**-MOF-1 **(1)** were collected at 298, 273 and 258 K.

**Molecular Simulation Study for Methane Storage.**

With the aim to gain a better understanding of the structure-properties relationship governing the resultant high methane storage capacities in the Al-**soc**-MOFs, we assessed theoretically the plausible $CH_4$ storage capacity of various plausible theoretical isoreticular Al-**soc**-MOFs, based on expanded and/or functionalized tetracarboxylate organic building blocks.

In order to derive a better correlation between the **soc**-MOF gas storage properties and the make-up of the **soc**-MOF porous system (pore shape and size, ligand dimensions and functionalities), a comprehensive molecular simulation study was carried out on various hypothetical/isoreticular Al-**soc**-MOFs constructed using hypothetical organic building blocks. Firstly, we envisioned to validate our molecular simulation methodology on the parent **1** (Al-**soc**-MOF-1) and corroborate the mechanistic of $CH_4$ adsorption at 5 bar and at higher pressures, resulting on the outstanding $CH_4$ working capacity. Secondly, simulate and evaluate the absolute and working $CH_4$ uptakes for various hypothetical isoreticular **soc**-MOFs, constructed using different optimized (i) elongated, (ii) functionalized and (iii) contracted organic MBBs. In effect, the simulated isoreticular Al-**soc**-MOFs were assembled using both experimentally synthesized and hypothetically designed linkers obtained by modifying the arms and/or the core of the Al-**soc**-MOF-1 ligand as shown in Figure 6, Figure S47 and Scheme S2, Supporting Information. Figures 6 depicts the naming scheme employed to label the hypothetical Al-**soc**-MOF linkers. For example, the original linker is shown in Figure 6 (left), where **P-P** means phenyl – phenyl: both arm and core have one phenyl group. While **PP-APA** stands for phenyl – phenyl for arm and acetylene – phenyl –acetylene for core as shown in Figure 6 (right). A total of 18 theoretical analogues were hypothetically assembled and their associated $CH_4$ adsorption isotherms were simulated. For clarity the new simulated Al-**soc**-MOF structures will be named and referred to using the linker name.

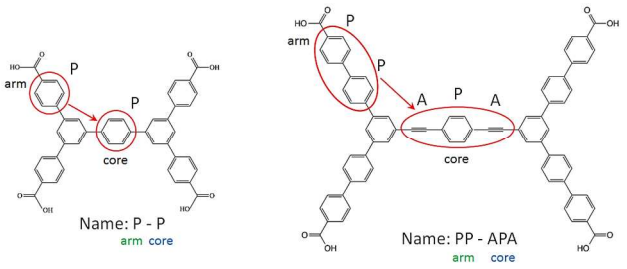


**Figure 6.** Scheme illustrating the adapted naming for the employed hypothetical organic ligands and associated hypothetical Al-**soc**-MOFs.

Initially, the Grand Canonical Monte Carlo (GCMC) simulations of methane adsorption were performed for the parent compound **1** in order to compare first the resulting simulated results with available experimental adsorption data and subsequently validate the simulation approach adopted in this study (Figure 7a and Figure S44, Supporting Information). More details about the employed simulation method is described in the Supporting Information. As shown, the theoretical $CH_4$ adsorption isotherm for the **P-P** is in a good agreement with the experimental data (**1**). The corresponding screenshots of methane adsorption at different relevant pressures, i.e. 5 bar (limiting desorption pressure) and 35, 65 and 80 (storage pressures) are shown in Figure 7b. The relatively very low simulated unused methane uptake at 5 bar (both gravimetric and volumetric) for **P-P** equivalent to **1**, at 5 bar, was confirmed by performing adsorption isotherms at different temperatures, namely at 298, 295, 273 and 258 K (Figure S45, Supporting Information). This is reflected in the observed non-preferential positions of $CH_4$ molecules in the framework of **P-P** (Figure 7b), .i.e. no specific preferential adsorption sites at 5 bar.

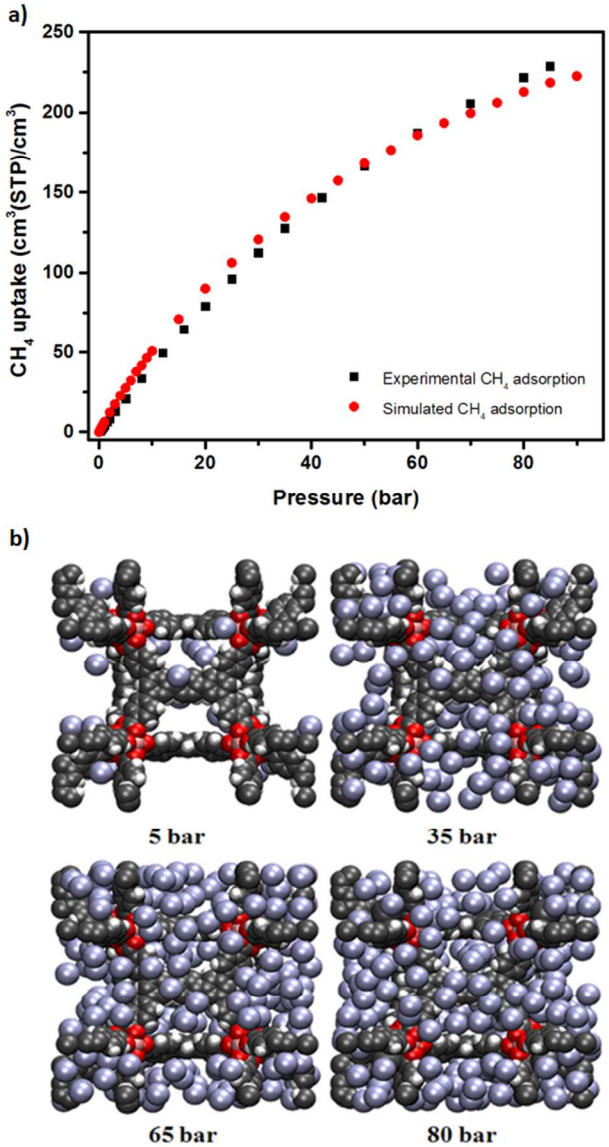


**Figure 7.** (a) Methane sorption in Al-**soc**-MOF-1 at 298 K: simulation (red filled circles) *vs.* experiment (black filled squares). (b) Screenshots of methane adsorption in **P-P** (equivalent to Al-**soc**-MOF-1) at 298 K at different pressure: 5, 35, 65 and 80 bar. The purple spheres surrounding the framework represent the methane molecules.

Delightfully, the simulated $CH_4$ adsorption isotherms on the optimized structure, based on molecular mechanics simulation approach (details in the Supporting Information.), of the parent **1** (**P-P**), is in a good agreement with the corresponding $CH_4$ adsorption isotherms simulated on the experimental structure (Figure S46, Supporting Information). Accordingly, the same

molecular mechanics optimization procedure was employed to construct 18 hypothetical isoreticular Al-**soc**-MOFs and subsequently simulate their associated total and working $CH_4$ uptakes using the GCMC approach.

The simulated absolute volumetric and gravimetric $CH_4$ adsorption isotherms for **P-P (1)** and the other isoreticular Al-**soc**-MOFs were simulated at various temperatures and up to 80 bar total pressure (Figures S76-S84, Supporting Information).

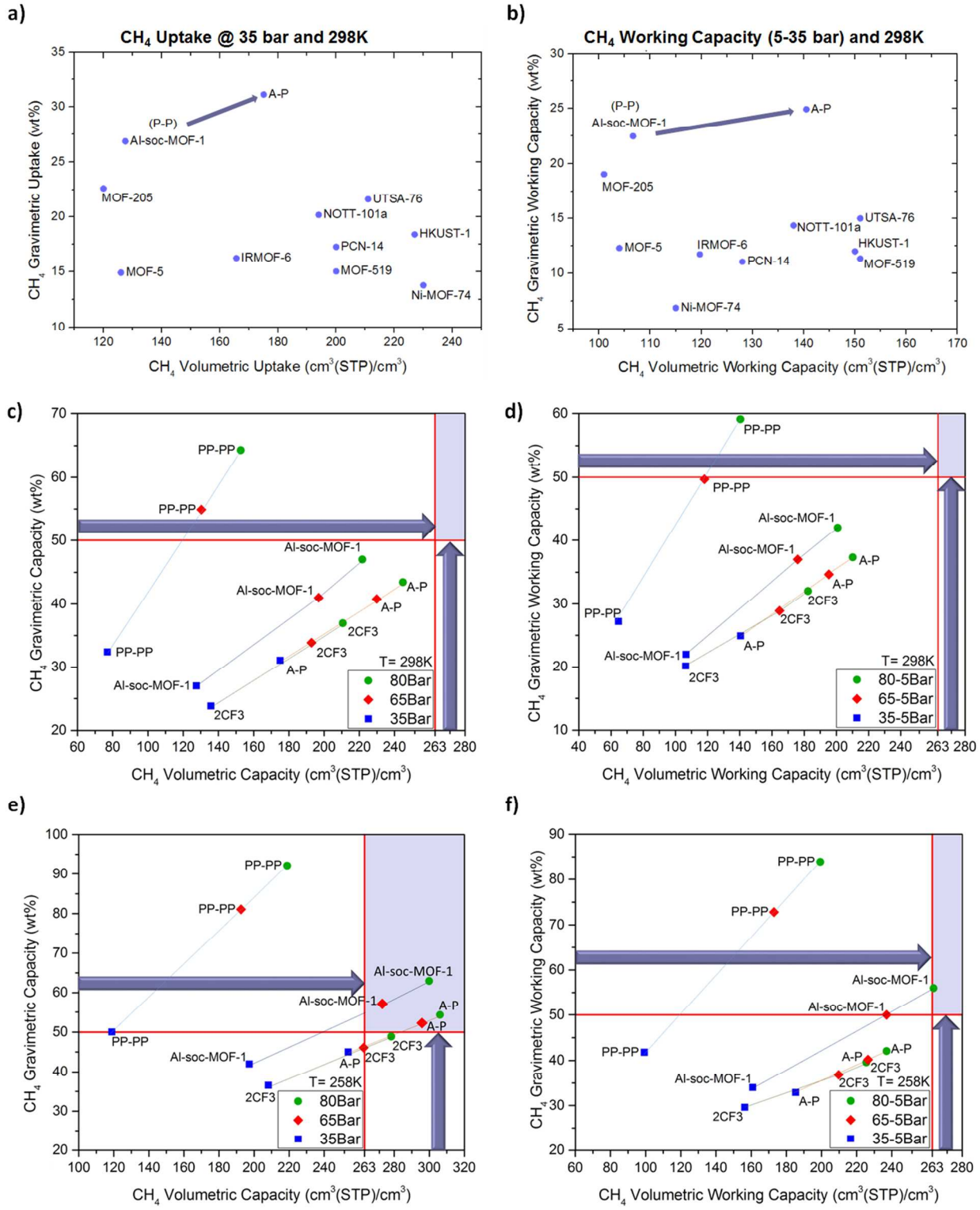


**Figure 8.** Total (a) at 35 bar and 5-35 bar working (b) $CH_4$ gravimetric and volumetric uptakes for P-P and A-P simulated structures as compared to the best MOF materials reported to date at 298 K. Theoretical total (left, c and e) and working (right, d and f) gravimetric vs. volumetric capacity for selected hypothetical isoreticular Al-**soc**-MOFs in a wide range of pressures (35, 65 and 80 bar) at different temperatures (298 and 258 K) as compared to Al-**soc**-MOF (**1**). The purple area represent the desired range of the best compromise between gravimetric and volumetric total and working uptakes.

Interestingly, these results showed that the use of (i) elongated, (ii) functionalized and (iii) contracted linkers resulted in three distinguished Al-**soc**-MOF groups in terms of gravimetric-volumetric uptake trade-off. In fact, the use of (i) elongated arms and/or cores, such as **PP-PP**, led to an increase in the gravimetric uptake at the expense of the volumetric uptake at any pressure and temperature conditions evaluated in this study. (ii) Functionalizing the phenyl core of the linker led generally to lower gravimetric uptake but still with good gravimetric-volumetric uptake trade-off at any pressure and temperature conditions explored here. In a particular case, strategies for functionalization of the phenyl cores with different functional groups, such as $CF_3$ and Br led to relatively good working volumetric uptake (due to the relatively higher framework density), albeit with much lower working gravimetric uptake. Interestingly, (iii) contraction of the arms and/or the core, for instance **A-P** structure, offer potential for a collective improvement (ideal compromise) of the gravimetric and volumetric uptakes as compared to **1** at any temperature, particularly at intermediate pressures of 35 bar (Figure 8). Principally, in terms of $CH_4$ working (5-35 bar) volumetric and gravimetric capacity trade-off, contraction of the arms showed a notable improvement in the absolute $CH_4$ uptake at 298 K. This unique compromise can be attributed to the enhanced $CH_4$ adsorption uptake at relatively high pressures below 35 bar, due to the reduced channel dimensions in the **A-P** structure as compared to the parent Al-**soc**-MOF-1 (9.3 Å x 10.0 Å vs 14.0 Å x 14.2 Å). It is important to note that the Al-**soc**-MOF-1 (**P-P**) still exhibits both enhanced volumetric and gravimetric trade-off for 5-65 bar and 5-80 bar working pressures at any temperature (Figure 8).

A summary of the theoretical results in terms of $CH_4$ absolute and working capacities, volumetric and gravimetric, at 298, 273 and 258 K in a wide range of pressures are presented in Figures S48-S66, Supporting Information.

### $O_2$ and $CO_2$ Storage Studies

The exceptional methane storage capabilities of Al-**soc**-MOF-1 have inspired us to extend this study to other important commodities, namely $O_2$ and $CO_2$. Accordingly, we recorded various $O_2$ and $CO_2$ adsorption isotherms for Al-**soc**-MOF-1. Noticeably, the amounts of $O_2$ and $CO_2$ adsorbed in Al-**soc**-MOF-1 near saturation pressures (0.95 $p/p_0$), derived from adsorption isotherms at 90.2 K and 195.15 K for $O_2$ and $CO_2$ respectively, were found to be remarkably high (1757 $cm^3$ (STP)/g and 1236 $cm^3$ (STP)/g, respectively) (Figure S29, Supporting Information). Markedly, the combination of experimentally accessible low pressure (at 90.2 K) and high pressure $O_2$ adsorption data up to 115 bar (at 298 K) (combined with Toth model) revealed that Al-**soc**-MOF-1 exhibits a record of 29 mmol/g absolute gravimetric $O_2$ uptake at 140 bar that is much higher than HKUST-1 (13.2 mmol/g) and NU-125 (17.4 mmol/g)[31], reference materials for the application (Figure 9).[15] Additionally, Al-**soc**-MOF-1 displayed a record deliverable capacity between 5 and 140 bar of 27.5 mmol/g vs 11.8 and 15.4 mmol/g for HKUST-1 and NU-**125** respectively (Figure 9a). Consequently by neglecting the effect of packing density and the void space occupied by the material, a 1 L cylinder filled with Al-**soc**-MOF-1 will potentially enhance the volumetric $O_2$ storage capacity (172 $cm^3/cm^3$) by 70% at 100 bar as compared to a conventional empty cylinder[32] (Figure 9b). It is to note that if we assume a prospective 25% loss associated to packing density, the Al-**soc**-MOF-1 volumetric $O_2$ storage capacity still offers a 25% enhancement over an empty cylinder. Analysis of the $O_2$ adsorption recorded at variable temperatures indicated that **1** exhibits a relatively low $O_2$ heat of adsorption (10 kJ/mol at low loading) in the whole $O_2$ loading range, slightly higher than the $O_2$ latent heat of evaporation (Figure S33, Supporting Information).

Additionally, the $CO_2$ adsorption studies revealed that Al-**soc**-MOF-1 exhibits an exceptional absolute gravimetric $CO_2$ uptake at 40 bar of 2 g/g (1020 $cm^3$ (STP)/g) *vs.* 1.5 g/g for MOF-177, a setting a new record among microporous MOFs (Figure S39, Supporting Information). Consequently, Al-**soc**-MOF-1 displays the uppermost working capacity between 1 bar and 40 bar of 1.90 g/g (967 $cm^3$ (STP)/g) vs 1.46 g/g (742 $cm^3$ (STP)/g) for MOF-177.[24b] The analysis of variable temperature $CO_2$ adsorption data showed that Al-**soc**-MOF-1 exhibits a relatively low $CO_2$ heat of adsorption (17 kJ/mol at low loading) in the whole $CO_2$ loading range (Figure S31b, Supporting Information). It is important to note that the mesoporous MOF-210[24b] exhibits the highest absolute gravimetric $CO_2$ uptake at 50 bar (2.8 g/g).

Finally, it is worth noting that Al-**soc**-MOF-1 exhibits also an excellent $H_2$ storage capacity at 77 K (ca. 11 wt %) (Figure S40, Supporting Information) at high pressure (30 bar) in comparison to other highly porous materials.

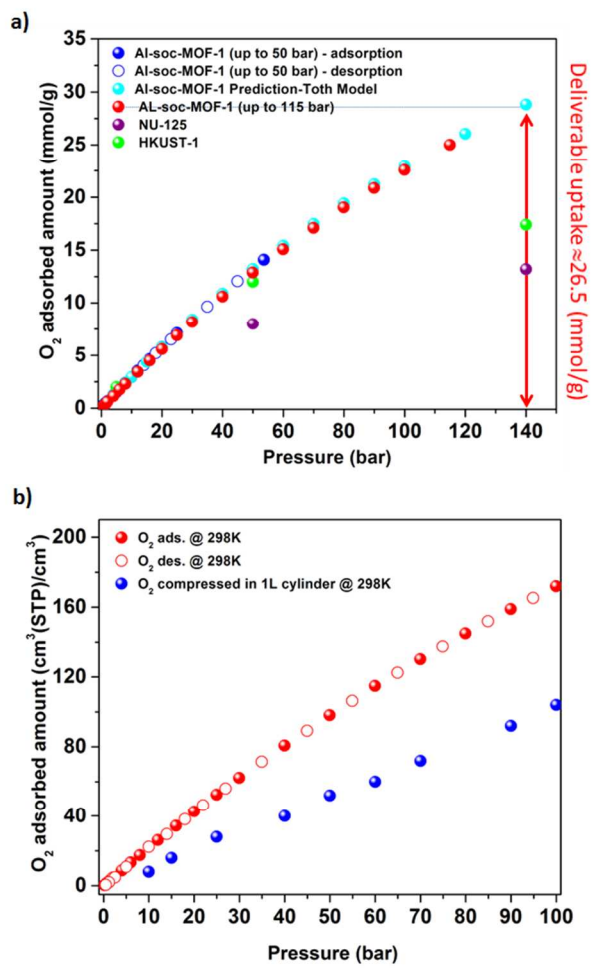


**Figure 9.** (a) Single component gravimetric gas adsorption isotherm for $O_2$ at 298 K showing that **1** exhibits the highest deliverable uptake reported so far. (b) Volumetric $O_2$ adsorption isotherm compared to the storage capacity in pressurized container.[32]

Similarly, $O_2$ and $CO_2$ adsorption studies were performed for the two isoreticular Al-**soc**-MOFs (**2** and **3)** and revealed that the naphthalene and anthracene analogues exhibit only a slightly lower $O_2$ and $CO_2$ adsorption uptakes under the same condition as compared to **1** (Figures S42, S43 and Table S4, Supporting Information).

## CONCLUSIONS

In summary, we successfully employed the molecular building block approach to synthesize the first aluminum **soc**-MOF isoreticular materials. Specifically, reaction conditions that consistently permit the *in-situ* generation of the $[Al_3(\mu_3\text{-}O)(H_2O)_6(O_2C{-})_6]$ MBB were isolated and used for the construction of a highly porous (4,6)-connected aluminum based **soc**-MOF, Al-**soc**-MOF-1 , with more than 6000 $m^2/g$ Langmuir specific surface area.

Importantly, the tedious activation using dry supercritical $CO_2$ is not required in order to activate the Al-**soc**-MOF-1 and its naphthalene and anthracene analogues. Particularly, the conventional activation technique, i.e. simple combination of heating and vacuum (or $N_2$ flush), is sufficient for the full activation prior gas loading-unloading cycles.

Extensive gas adsorption studies were carried out on the Al-**soc**-MOF platform with different gases ($N_2$, $CO_2$, $CH_4$, $O_2$, *etc*.). Methane adsorption isotherms were completed at different temperatures and in a wide range of pressures up to 85 bar. Interestingly, it was found that Al-**soc**-MOF-1 exhibits one of the highest total and working gravimetric $CH_4$ uptakes at 35 bar. In contrast to other reported best MOFs for $CH_4$ storage, Al-**soc**-MOF-1 showed enhanced $CH_4$ storage working capacity as the temperature is decreased. Particularly, at 258 K and 80 bar, the Al-**soc**-MOF-1 fulfils the DOE target and exhibits the highest working volumetric capacity of 264 $cm^3(STP)/cm^3$. To the best of our knowledge, this is the first time that a porous material fulfills both the challenging gravimetric and volumetric targets for the $CH_4$ working capacity. The collective experimental and GCMC simulation studies indicated that the parent Al-**soc**-MOF-1, in contrast to various hypothetical isoreticular Al-**soc**-MOFs based on contracted, elongated and functionalized ligands, exhibits the best compromise between the volumetric and gravimetric total and working uptakes in a wide range of pressure and temperature conditions.

## EXPERIMENTAL SECTION

**Materials and methods.** Details on the synthesis of the organic ligands used in this study, 3,3",5,5"-tetrakis(4-carboxyphenyl)-p-terphenyl ($H_4$TCPT), 3',3",5',5"-tetrakis(4-carboxyphenyl)-1,4-diphenylnaphthalene (TCDPN) and 3',3",5',5"-tetrakis(4-carboxyphenyl)-9,10-diphenylanthracene (TCDPA)[19] are provided in the Supporting Information.

Single-crystal diffraction data were collected at beamline I19, Diamond Light Source, Didcot, UK using a wavelength $\lambda$ = 1.0402 Å at 250 K. Fourier-transform infrared (FT-IR) spectra (4000−600 $cm^{-1}$) were collected in the solid state on a Nicolet 700 FT-IR spectrometer. The peak intensities are described in each of the spectra as very strong (vs), strong (s), medium (m), weak (w), broad (br) and shoulder (sh). Powder X-ray diffraction (PXRD) measurements were performed on a PANalytical MPD X'Pert PRO X-ray diffractometer at 45 kV, 40 mA for Cu K$\alpha$ ($\lambda$ = 1.5418 Å) equipped with a variable-temperature stage, with a scan speed of 20/min. The sample was held at the designated temperature for at least 10 min between each scan. High resolution dynamic thermal gravimetric analysis (TGA) were performed under a continuous $N_2$ flow and recorded on a TA Instruments hi-res TGAQ500 thermogravimetric analyzer. Low pressure gas sorption measurements were performed on a fully automated Autosorb-1C gas sorption analyzer (Quantachrome Instruments). High pressure gas sorption studies were performed on a magnetic suspension balance marketed by Rubotherm (Germany).

**Synthesis of Al-**soc**-MOF-1**: A solution of $AlCl_3.6H_2O$ (29 mg, 0.015 mmol), **$H_4$L1** (7.1 mg, 0.01 mmol), in N,N-dimethylformamide (DMF) (1 ml), acetonitrile ($CH_3CN$) (1 ml) and nitric acid (3.5 M, 0.5 ml) was prepared in a 20-ml scintillation vial and subsequently placed into preheated oven at 130˚C for 12 h to give pure small colorless cube-shaped crystals. Suitable single crystals were obtained using the same synthetic procedure, but with increasing the amount of $HNO_3$ to 1 ml. Crystals of Al-**soc**-MOF-1 were harvested, washed with $CH_3CN$ and air-dried. FT-IR (4000 - 650 $cm^{-1}$): 3349 (br), 1605 (s), 1592 (s), 1423 (s), 1387 (vs), 1312 (w), 1243 (w), 1100 (w), 1018 (w), 854 (w), 830 (w), 783 (s), 771 (s).701(s).

**Synthesis of Al-**soc**-MOF-2**: A solution of $AlCl_3.6H_2O$ (29 mg, 0.015 mmol), **$H_4$L2** (7.6 mg, 0.01 mmol), in N,N-dimethylformamide (DMF) (1 ml), acetonitrile ($CH_3CN$) (1 ml) and nitric acid (3.5 M, 0.5 ml) was prepared in a 20-ml scintillation vial and subsequently placed into preheated oven at 130˚C for 12 h to give pure small colorless cube-shaped crystals. Suitable single crystals were obtained using the same synthetic procedure, but with increasing the amount of $HNO_3$ to 1 ml. Crystals of Al-**soc**-MOF-2 were harvested, washed with $CH_3CN$ and air-dried. FT-IR (4000 - 650 $cm^{-1}$): 3349 (br), 1606 (s), 1545 (m), 1422 (s), 1384 (s), 1241 (w), 1100 (w), 1015 (w), 851 (w), 851 (w), 771 (s).705(m).

**Synthesis of Al-**soc**-MOF-3**: A solution of $AlCl_3.6H_2O$ (29 mg, 0.015 mmol), **$H_4$L3** (8.1 mg, 0.01 mmol), in N,N-dimethylformamide (DMF) (1 ml), acetonitrile ($CH_3CN$) (1 ml) and nitric acid (3.5 M, 0.3 ml) was prepared in a 20-ml scintillation vial and subsequently placed into preheated oven at 130˚C for 12 h to give pure microcrystalline yellow powder. Suitable single crystals were obtained using the same synthetic procedure, but with increasing the amount of $HNO_3$ to 1 ml. Crystals of Al-**soc**-MOF-3 were harvested, washed with $CH_3CN$ and air-dried. FT-IR (4000 - 650 $cm^{-1}$): 3349 (br), 1606 (s), 1547 (s), 1442 (s), 1387 (s), 1312 (w), 1241 (w), 1181 (w), 1016 (w), 852 (m), 771 (s), 706 (s).

## ASSOCIATED CONTENT

### Supporting Information

Synthesis of organic ligands, PXRD, additional structural figures, sorption, and single-crystal X-ray diffraction data (CIF). This material is available free of charge via the Internet at http://pubs.acs.org

## AUTHOR INFORMATION

### Corresponding Author

mohamed.eddaoudi@kaust.edu.sa

### Notes

The authors declare no competing financial interests.

## ACKNOWLEDGMENT

Research reported in this publication was supported by King Abdullah University of Science and Technology (KAUST). The authors thank Diamond Light Source for access to

beamline I19 (MT10189) that contributed to the results presented here and also D. Allan and H. Nowell for their assistance during the measurements.

## REFERENCES

(1) (a) Morris, R. E.; Wheatley, P. S. *Angew. Chem., Int. Ed.* **2008**, *47*, 4966-4981. (b) Suh, M. P.; Park, H. J.; Prasad, T. K.; Lim, D.-W. *Chem. Rev.* **2011**, *112*, 782-835. (c) Li, T.; Chen, D.-L.; Sullivan, J. E.; Kozlowski, M. T.; Johnson, J. K.; Rosi, N. L. *Chem. Sci.* **2013**, *4*, 1746-1755.

(2) (a) He, Y.; Zhou, W.; Qian, G.; Chen, B. *Chem. Soc. Rev.* **2014**, *43*, 5657-5678. (b) Eddaoudi, M.; Kim, J.; Rosi, N.; Vodak, D.; Wachter, J.; O'Keeffe, M.; Yaghi, O. M. *Science* **2002**, *295*, 469-472. (c) Konstas, K.; Osl, T.; Yang, Y.; Batten, M.; Burke, N.; Hill, A. J.; Hill, M. R. *J. Mater. Chem.* **2012**, *22*, 16698-16708.

(3) Lozano-Castelló, D.; Alcañiz-Monge, J.; de la Casa-Lillo, M. A.; Cazorla-Amorós, D.; Linares-Solano, A. *Fuel* **2002**, *81*, 1777-1803.

(4) Wegrzyn, J.; Gurevich, M. *Appl. Energy* **1996**, *55*, 71-83.

(5) (a) Menon, V. C.; Komarneni, S. *J. Porous Mater.* **1998**, *5*, 43-58. (b) Düren, T.; Sarkisov, L.; Yaghi, O. M.; Snurr, R. Q. *Langmuir* **2004**, *20*, 2683-2689.

(6) (a) Gándara, F.; Furukawa, H.; Lee, S.; Yaghi, O. M. *J. Am. Chem. Soc.* **2014**, *136*, 5271-5274. (b) Wilmer, C. E.; Farha, O. K.; Yildirim, T.; Eryazici, I.; Krungleviciute, V.; Sarjeant, A. A.; Snurr, R. Q.; Hupp, J. T. *Energy Environ. Sci.* **2013**, *6*, 1158-1163.

(7) (a) Liu, J.; Thallapally, P. K.; McGrail, B. P.; Brown, D. R.; Liu, J. *Chem. Soc. Rev.* **2012**, *41*, 2308-2322. (b) Sumida, K.; Rogow, D. L.; Mason, J. A.; McDonald, T. M.; Bloch, E. D.; Herm, Z. R.; Bae, T.-H.; Long, J. R. *Chem. Rev.* **2011**, *112*, 724-781. (c) Wheatley, P. S.; McKinlay, A. C.; Morris, R. E., Gédéon, A.; Babonneau, F. *Stud. Surf. Sci. Catal.* **2008**, *174*, 441– 446.

(8) (a) McKinlay, A. C.; Eubank, J. F.; Wuttke, S.; Xiao, B.; Wheatley, P. S.; Bazin, P.; Lavalley, J. C.; Daturi, M.; Vimont, A.; De Weireld, G.; Horcajada, P.; Serre, C.; Morris, R. E. *Chem. Mater.* **2013**, *25*, 1592-1599. (b) Wheatley, P. S.; Butler, A. R.; Crane, M. S.; Fox, S.; Xiao, B.; Rossi, A. G.; Megson, I. L.; Morris, R. E. *J. Am. Chem. Soc.* **2005**, *128*, 502-509. (c) Zhang, H.; Annich, G. M.; Miskulin, J.; Stankiewicz, K.; Osterholzer, K.; Merz, S. I.; Bartlett, R. H.; Meyerhoff, M. E. *J. Am. Chem. Soc.* **2003**, *125*, 5015-5024.

(9) Wang, Y.; Helvensteijn, B.; Nizamidin, N.; Erion, A. M.; Steiner, L. A.; Mulloth, L. M.; Luna, B.; LeVan, M. D. *Langmuir* **2011**, *27*, 10648-10656.

(10) McGovern, S. J.; Yeigh, J. H. FCC Regeneration. U.S. Patent 4,370,222 A, Jan 25, 1983.

(11) (a) Furukawa, H.; Cordova, K. E.; O'Keeffe, M.; Yaghi, O. M. *Science* **2013**, *341*. (b) Cook, T. R.; Zheng, Y.-R.; Stang, P. J. *Chem. Rev.* **2012**, *113*, 734-777. (c) McKinlay, A. C.; Morris, R. E.; Horcajada, P.; Férey, G.; Gref, R.; Couvreur, P.; Serre, C. *Angew. Chem., Int. Ed.* **2010**, *49*, 6260-6266. (d) Ferey, G. *Chem. Soc. Rev.* **2008**, *37*, 191-214. (e) Zhou, H.-C.; Long, J. R.; Yaghi, O. M. *Chem. Rev.* **2012**, *112*, 673-674. (f) Shekhah, O.; Belmabkhout, Y.; Chen, Z.; Guillerm, V.; Cairns, A.; Adil, K.; Eddaoudi, M. *Nat. Commun.* **2014**, *5*, 4228. (g) Nugent, P.; Belmabkhout, Y.; Burd, S. D.; Cairns, A. J.; Luebke, R.; Forrest, K.; Pham, T.; Ma, S.; Space, B.; Wojtas, L.; Eddaoudi, M.; Zaworotko, M. J. *Nature* **2013**, *495*, 80-84. (h) Belmabkhout, Y.; Mouttaki, H.; Eubank, J. F.; Guillerm, V.; Eddaoudi, M. *RSC Adv.* **2014**, *4*, 63855-63859.

(12) (a) Seidel, S. R.; Stang, P. J. *Acc. Chem. Res.* **2002**, *35*, 972-983. (b) Yaghi, O. M.; O'Keeffe, M.; Ockwig, N. W.; Chae, H. K.; Eddaoudi, M.; Kim, J. *Nature* **2003**, *423*, 705-714. (c) Eddaoudi, M.; Sava, D. F.; Eubank, J. F.; Adil, K.; Guillerm, V. *Chem. Soc. Rev.* **2015**, *44*, 228-249. (d) Guillerm, V.; Kim, D.; Eubank, J. F.; Luebke, R.; Liu, X.; Adil, K.; Lah, M. S.; Eddaoudi, M. *Chem. Soc. Rev.* **2014**, *43*, 6141-6172. (e) Eddaoudi, M.; Moler, D. B.; Li, H.; Chen, B.; Reineke, T. M.; O'Keeffe, M.; Yaghi, O. M. *Acc. Chem. Res.* **2001**, *34*, 319-330. (f) Xue, D.-X.; Cairns, A. J.; Belmabkhout, Y.; Wojtas, L.; Liu, Y.; Alkordi, M. H.; Eddaoudi, M. *J. Am. Chem. Soc.* **2013**, *135*, 7660-7667.

(13) Chae, H. K.; Siberio-Perez, D. Y.; Kim, J.; Go, Y.; Eddaoudi, M.; Matzger, A. J.; O'Keeffe, M.; Yaghi, O. M. *Nature* **2004**, *427*, 523-527.

(14) (a) Liu, Y.; Eubank, J. F.; Cairns, A. J.; Eckert, J.; Kravtsov, V. C.; Luebke, R.; Eddaoudi, M. *Angew. Chem., Int. Ed.* **2007**, *46*, 3278-3283. (b) Pang, M.; Cairns, A. J.; Liu, Y.; Belmabkhout, Y.; Zeng, H. C.; Eddaoudi, M. *J. Am. Chem. Soc.* **2012**, *134*, 13176-13179.

(15) Feng, D.; Wang, K.; Wei, Z.; Chen, Y.-P.; Simon, C. M.; Arvapally, R. K.; Martin, R. L.; Bosch, M.; Liu, T.-F.; Fordham, S.; Yuan, D.; Omary, M. A.; Haranczyk, M.; Smit, B.; Zhou, H.-C. *Nat. Commun.* **2014**, *5*, 5723.

(16) Peng, Y.; Krungleviciute, V.; Eryazici, I.; Hupp, J. T.; Farha, O. K.; Yildirim, T. *J. Am. Chem. Soc.* **2013**, *135*, 11887-11894.

(17) Mueller, U.; Schubert, M.; Teich, F.; Puetter, H.; Schierle-Arndt, K.; Pastre, J. *J. Mater. Chem.* **2006**, *16*, 626-636.

(18) (a) Volkringer, C.; Popov, D.; Loiseau, T.; Férey, G.; Burghammer, M.; Riekel, C.; Haouas, M.; Taulelle, F. *Chem. Mater.* **2009**, *21*, 5695-5697. (b) Devic, T.; Serre, C. *Chem. Soc. Rev.* **2014**, *43*, 6097-6115. (c) Serra-Crespo, P.; Ramos-Fernandez, E. V.; Gascon, J.; Kapteijn, F. *Chem. Mater.* **2011**, *23*, 2565-2572. (d) Loiseau, T.; Lecroq, L.; Volkringer, C.; Marrot, J.; Férey, G.; Haouas, M.; Taulelle, F.; Bourrelly, S.; Llewellyn, P. L.; Latroche, M. *J. Am. Chem. Soc.* **2006**, *128*, 10223-10230. (e) Feng, D.; Liu, T.-F.; Su, J.; Bosch, M.; Wei, Z.; Wan, W.; Yuan, D.; Chen, Y.-P.; Wang, X.; Wang, K.; Lian, X.; Gu, Z.-Y.; Park, J.; Zou, X.; Zhou, H.-C. *Nat. Commun.* **2015**, *6*, 5979.

(19) Luebke, R.; Belmabkhout, Y.; Weselinski, L. J.; Cairns, A. J.; Alkordi, M.; Norton, G.; Wojtas, L.; Adil, K.; Eddaoudi, M. *Chem. Sci.* **2015**, *6*, 4095-4102.

(20) (a) O'Keeffe, M.; Eddaoudi, M.; Li, H.; Reineke, T.; Yaghi, O. M. *J. Solid State Chem.* **2000**, *152*, 3-20. (b) O'Keeffe, M.; Peskov, M. A.; Ramsden, S. J.; Yaghi, O. M. *Acc. Chem. Res.* **2008**, *41*, 1782-1789.

(21) Li, M.; Li, D.; O'Keeffe, M.; Yaghi, O. M. *Chem. Rev.* **2013**, *114*, 1343-1370.

(22) LeBail, A.; Duroy, H.; Fourquet, J. L. *Mat. Res. Bull.* **1988**, *23*, 447-452.

(23) Spek, A. L. *Acta Crystallogr.* **1990**, A46, c34.

(24) (a) Nelson, A. P.; Farha, O. K.; Mulfort, K. L.; Hupp, J. T. *J. Am. Chem. Soc.* **2008**, *131*, 458-460. (b) Furukawa, H.; Ko, N.; Go, Y. B.; Aratani, N.; Choi, S. B.; Choi, E.; Yazaydin, A. Ö.; Snurr, R. Q.; O'Keeffe, M.; Kim, J.; Yaghi, O. M. *Science* **2010**, *329*, 424-428. (c) Farha, O. K.; Özgür Yazaydın, A.; Eryazici, I.; Malliakas, C. D.; Hauser, B. G.; Kanatzidis, M. G.; Nguyen, S. T.; Snurr, R. Q.; Hupp, J. T. *Nature Chem.* **2010**, *2*, 944-948.

(25) Stoeck, U.; Krause, S.; Bon, V.; Senkovska, I.; Kaskel, S. *Chem. Commun.* **2012**, *48*, 10841-10843.

(26) Li, B.; Wen, H.-M.; Wang, H.; Wu, H.; Tyagi, M.; Yildirim, T.; Zhou, W.; Chen, B. *J. Am. Chem. Soc.* **2014**, *136*, 6207-6210.

(27) (a) Chui, S. S.-Y.; Lo, S. M.-F.; Charmant, J. P. H.; Orpen, A. G.; Williams, I. D. *Science* **1999**, *283*, 1148-1150. (b) Mason, J. A.; Veenstra, M.; Long, J. R. *Chem. Sci.* **2014**, *5*, 32-51.

(28) Rosi, N. L.; Kim, J.; Eddaoudi, M.; Chen, B.; O'Keeffe, M.; Yaghi, O. M. *J. Am. Chem. Soc.* **2005**, *127*, 1504-1518.

(29) Peng, Y.; Srinivas, G.; Wilmer, C. E.; Eryazici, I.; Snurr, R. Q.; Hupp, J. T.; Yildirim, T.; Farha, O. K. *Chem. Commun.* **2013**, *49*, 2992-2994.

(30) Ma, S.; Sun, D.; Simmons, J. M.; Collier, C. D.; Yuan, D.; Zhou, H.-C. *J. Am. Chem. Soc.* **2007**, *130*, 1012-1016.

(31) DeCoste, J. B.; Weston, M. H.; Fuller, P. E.; Tovar, T. M.; Peterson, G. W.; LeVan, M. D.; Farha, O. K. *Angew. Chem., Int. Ed.* **2014**, *53*, 14092-14095.

(32) Zhou, Y.; Wei, L.; Yang, J.; Sun, Y.; Zhou, L. *J. Chem. Eng. Data* **2005**, *50*, 1068-1072.

**TOC**

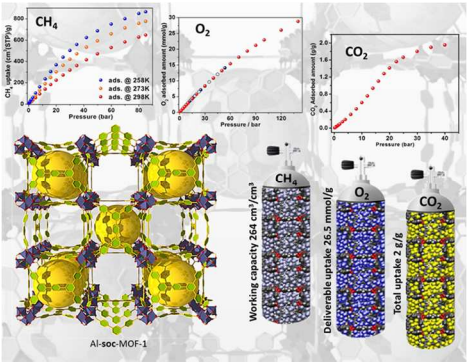
CH4
O2
CO2
Pressure (bar)
Pressure / bar
ads. @ 258K
ads. @ 273K
ads. @ 298K
Al-soc-MOF-1
Working capacity 264 cm³/cm³
Deliverable uptake 26.5 mmol/g
Total uptake 2 g/g

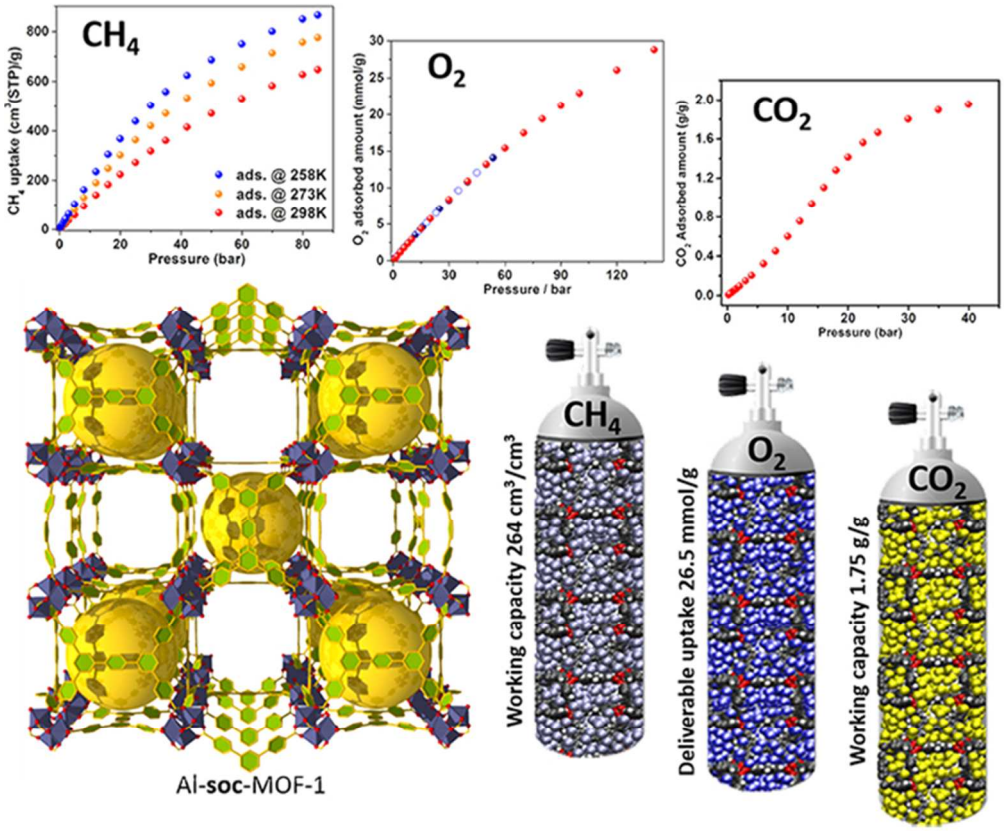


70x58mm (300 x 300 DPI)